Separation and Purification Technology 356 (2025) 129947

Contents lists available at ScienceDirect

Separation and Purification Technology

journal homepage: www.elsevier.com/locate/seppur

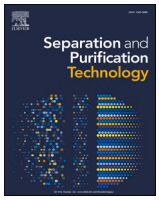

Insights into the mixing effect in organic solvent nanofiltration from simulations on covalent organic frameworks (COFs)

Shukai Li [a], Bowen Liu [a], Mingjie Wei [a,*], Ming Liu [a], Jinji Cao [a], Weihong Xing [a], Yong Wang [a,b,*]

[a] State Key Laboratory of Materials-Oriented Chemical Engineering, College of Chemical Engineering, Nanjing Tech University, Nanjing 211816, Jiangsu, China
[b] School of Energy and Environment, Southeast University, Nanjing 210096, Jiangsu, China

ARTICLE INFO

Keywords:
Transport mechanism
Mixed solvents
Ideal selectivity
Real selectivity

ABSTRACT

Low-energy organic solvent separation is crucial for the petrochemical industry. Covalent organic framework (COF) membranes hold immense promise for rapid separation of organic solvents. Understanding of the transport mechanisms of solvents is critical for COF-membrane design. In this study, molecular dynamics simulations are employed to investigate the separation behaviors of three most extensively used solvents (methanol, ethanol, and acetone) and their mixtures on COF membranes. It is found that despite high ideal selectivity, real selectivity approaches to 1, primarily due to in-pore transport effects, notably enhanced flow rates of ethanol in mixed-solvent cases. Subsequently, mixing effect is explored from molecular analysis. It is revealed that no clear evidence of preferential adsorption for methanol or acetone based on density distribution results. Calculation of self-diffusion coefficients indicates that the mobility of ethanol is evidently promoted in the mixed-solvent conditions, caused by the attraction between ethanol molecules is reduced because of the coexistence of other solvent molecules. The unexpectedly promoted permeance of ethanol in mixed-solvent cases consequently lowers the selectivity. Results in this work highlight the solvent–solvent interactions as crucial factors influencing separation performance and provide knowledge of membrane design for highly efficient separations of organic solvents.

1. Introduction

In the chemical industrial, separation processes are responsible for about 50 % of global energy consumption [1]. The separation of organic solvents is particularly crucial, but traditional thermal separation technologies such as distillation encounter limitations due to high carbon emissions and inefficiencies when handling complex organic solvent systems, including azeotropes, isomers, and thermally sensitive compounds [2]. Consequently, membrane separation technologies have garnered significant attention for their potential to address these challenges through enhanced energy efficiency, environmental sustainability, and operational simplicity [3].

Various membrane processes have been developed for organic solvent systems, including organic solvent nanofiltration (OSN), pervaporation, organic solvent reverse osmosis, and organic solvent forward osmosis [4]. Among these, OSN technology stands out for organic solvent separation due to its mild operational conditions and high flux capabilities, making it well-suited for pharmaceutical and large-scale chemical applications [5–8]. However, OSN membranes face challenges in complex environments [4,9–11], necessitating high stability and solvent resistance. Currently, most membranes used in OSN applications are polymer-based [6,12]. Their selectivity and permeability performance require further enhancement to meet practically economical demands [13].

As an emerging porous material, covalent organic frameworks (COFs) feature ordered networks, high crystallinity as well as flexibility on chemical modification, low density, large surface area, facilely-tailored functionalities and exhibit thermal and chemical stability in aqueous and solvent environments [14,15]. Among them, the separation application of COFs is attracting particular attention due to the distinct structural features of COFs and facile membrane formation. Therefore, they are pivotal for applications in membrane technology [16]. Mishra *et al.* synthesized COF membranes through liquid–liquid interfacial polymerization, exhibiting excellent Congo Red retention properties [17]. Yin *et al.* developed a thin-film nanocomposite membrane of COFs-polyamide, which exhibits exceptional solvent resistance and high drug

* Corresponding authors.
E-mail addresses: mj.wei@njtech.edu.cn (M. Wei), yongwang@seu.edu.cn (Y. Wang).

https://doi.org/10.1016/j.seppur.2024.129947
Received 19 August 2024; Received in revised form 23 September 2024; Accepted 30 September 2024
Available online 30 September 2024

molecule retention rates [18]. Zhu *et al.* investigated the transport and separation mechanism of dye in TpPa-1[19]. Zhang *et al.* utilized an in-situ molecular welding approach to fabricate defect-free COF membranes [20], demonstrating high permeability to solvents such as ethanol, methanol, acetone, hexane, and acetonitrile, with retention rates exceeding 95 % for various dyes.

The permeance correlates with both COF properties and solvent characteristics [21]. For instance, Xu *et al.* demonstrated that grafting groups significantly affects the hydrophilic/hydrophobic properties of COFs [22], while Wei *et al.* showed that hydrophobic COF membranes would enhance solvent flux [11]. Moreover, Wang *et al.* changed the adsorption performance of COF on bisphenol A by grafting different groups on COF [23]. The abundant types of solvent and COF make it extremely difficult to screening out the suitable COFs for specific solvent–solvent separations. Understanding the mechanism of solvent transport through COF membranes will help to narrow the range of COF candidates and to design new types of COFs.

In this study, non-equilibrium molecular dynamics (NEMD) simulations are employed to measure the fluxes of methanol, ethanol, and acetone, which are common in industrial solvent–solvent separations, through COF membranes. The TpPa, as well as those functionalized with various grafting groups (denoted as TpPa-R), are selected as COF membranes because this type of COF is mostly applied in the practical separations of solvent-related separations [24]. We firstly examine the transport behavior of pure solvents in TpPa-R membranes featuring different hydrophilic/hydrophobic properties and calculate the ideal selectivity based on the permeance data of pure solvents. Then, the ideal selectivity is compared with the real selectivity, which is calculated by data from simulations of mixed solvents. The alteration between real selectivity and ideal selectivity is observed. By the analysis of pore-entrance sieving effect and in-pore transport effect, we uncover the reason for the change of selectivity. Unlike most water treatment process in which the COF membranes play an important role, the solvent–solvent interaction in the present case should be adequately concerned while the grafting groups of TpPa-R takes little effect.

2. Simulation details

We utilized two primary models to simulate the separation of methanol/ethanol or acetone/ethanol mixtures by COF membranes. The first model consisted of a case where the COF was centrally positioned within a simulation box, flanked by two pure solvent boxes. The dimensions of the simulation box measured 3.9 nm and 4.5 nm in the x and y directions, respectively. To maintain solvent phase densities equivalent to real conditions, the dimensions in the z direction varied for each case. For the purpose of calculating the real selectivity, the mixed-solvent cases should be performed. The second model of mixed-solvent cases was then built within a box identical in dimensions to the first model in the x and y directions, but replacing the pure solvent boxes with mixed-solvent boxes. In the mixed-solvent case, the total amount of solvent molecules in the case is 1600, and each solvent is 800 molecules. The molar ratio of 1:1 is selected for binary solvents. Such molar ratio can reduce the error caused by the uneven local solvent concentration in the simulation and make the simulation results more representative. Similarly, the dimensions in the z direction varied to match ideal solvent densities. Fig. 1 illustrated the simulation model employing TpPa-H for the separation of methanol/ethanol mixtures.

All molecular dynamics simulations were conducted using the Large-scale Atomic/Molecular Massively Parallel Simulator (LAMMPS) software [25]. Non-bonded interactions between atoms were described using the Lennard-Jones (LJ) potential [26], with a cutoff radius of 1.0 nm for LJ interactions and 1.2 nm for electrostatic interactions. Long-range electrostatic interactions beyond the cutoff radius were computed using the Particle-Particle Particle-Mesh (PPPM) algorithm with a precision of 10^{-4}. COFs were modeled using the DREIDING force field [27], which is commonly used for COF simulations due to its simplicity and flexibility [28–30]. Solvent molecules were modeled with the AMBER-CORNELL [31] force field, known for its accuracy and reliability in organic systems. Charges on TpPa-R were computed using the Qeq [32] method, while solvent charges were derived from Restrained ElectroStatic Potential [33] (RESP) calculations based on Gaussian 09 results, with the Multiwfn software [34] used for processing. All pore size of TpPa-R can be calculated by Zeo++[35], the pore sizes of the four COFs TpPa-H, TpPa-NH_2, TpPa-SO_3H and TpPa-COOH are 15.82 Å,13.98661 Å,13.06032 Å and 10.86508 Å, respectively.

Prior to NEMD simulations, a 0.3 ns NPT (isothermal-isobaric) ensemble was used to thermodynamically equilibrate the simulation systems. NEMD simulations were then conducted using a pump method [36,37]. In this method, a constant pressure difference ΔP was applied across a 1 nm thick region along the z-axis, which served as the force region for all solvent molecules, exerting a fixed force f. This pressure difference ΔP acted as the driving force for membrane processes and was calculated as follows:

$$\Delta P = \frac{n \bullet f}{A} \tag{1}$$

where, ΔP is the transmembrane pressure difference in Pa; n is the number of solvent molecules within the force region; f is the specific force applied to each solvent molecule in Newtons; and A is the cross-sectional area of the membrane in the xy plane in m^2.

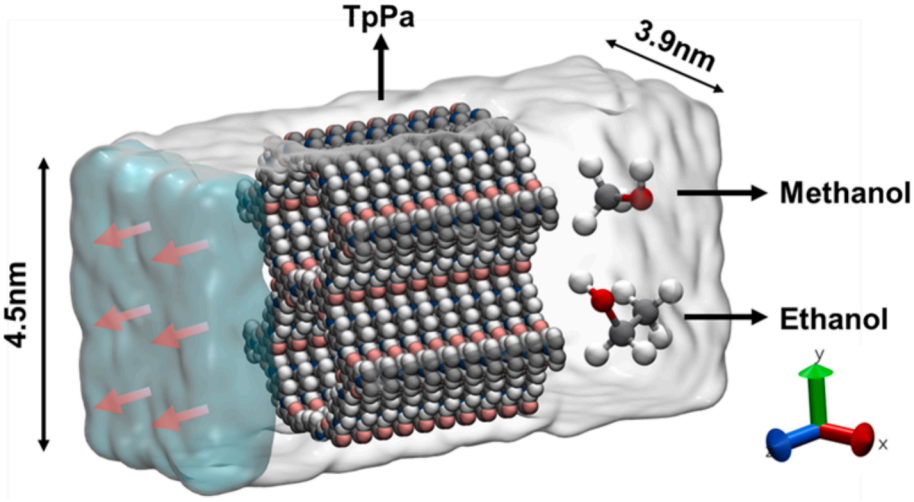

Fig. 1. The schematic diagram of simulation on the membrane separation process of methanol/ethanol mixture in the TpPa-H membrane.

The large ΔP (100 MPa) used in the NEMD simulations were higher than the experiments, to ensure rapid attainment of a steady-state process for subsequent data analysis [38]. Temperature was maintained around 300 K using Berendsen thermostats applied to the solvent molecules, regulating the system's kinetic energy and avoiding excessive external pressure input that could elevate system energy. NEMD simulations were conducted over 4 ns with a time step of 1 fs. The initial 1 ns was dedicated to system equilibration, while the subsequent 3 ns were used for flux calculations and detailed statistical analysis.

3. Results and discussions

3.1. Pure and mixed solvent fluxes

During NEMD simulations, the cumulative number of solvent molecules passing through the simulation box over time are initially recorded to compute the solvent flux (shown in Fig. S1). After that, the fluxes of solvents can be calculated by establishing the average number of solvent molecules across the membranes simulation system per nanosecond. Since the dependence of cumulative number of solvent molecules on simulation time are almost linear, it is easy to calculate the fluxes by the slops of each curve in Fig. S1, followed by unit conversions. The flux results are shown in Fig. 2a. Overall, the solvent fluxes through TpPa-H exhibits the highest as the ungrafted COF has the largest pore size. The fluxes through TpPa-NH_2 are slightly lower than those of TpPa-H because the lower transport resistance due to the nature of $-NH_2$ groups. The fluxes of solvents in TpPa-SO_3H and TpPa-COOH are obviously lower than the other two because of the shrunken pore size and higher transport resistance of $-SO_3H$ and –COOH groups. Similar dependence of solvent fluxes on grafted COFs is consistent with the experimental report [24].

The fluxes of various solvents are then compared. Regardless of the types of TpPa-R, the fluxes of methanol are evidently the highest while the fluxes of ethanol are the lowest. The distinct fluxes of methanol (or acetone) to ethanol indicates the ideal separation of methanol/ethanol (or acetone/ethanol). Before performing the simulations of mixed solvents, we prefer to figure out the reason behind variations of fluxes for distinct solvents.

The number and flow rate of solvent molecules inside all TpPa-R membranes are then calculated, and the results are illustrated in Fig. 2b-d. Comparing Fig. 2d with 2b, the numbers of methanol inside each TpPa-R membranes are obviously larger than those of ethanol. It is in accordance with the expectation that the pore of TpPa-R can contain more molecules with lower molecular weight, in other words, larger molar density in nanopores for solvents of lower molecular weight. Moreover, the methanol molecules move faster than ethanol molecules. The larger molar density and faster flow rate of methanol molecules inside TpPa-R nanopores result in the higher fluxes compared to ethanol.

However, the molecular weight of acetone is larger than that of ethanol, result in the lower molecular density inside membranes (shown in Fig. 2c). The larger flux of acetone should originate from the obvious higher flow rates compared to ethanol. Therefore, it can be expected that the flow rates of solvent molecules is also a crucial factor influencing solvent flux inside TpPa-R membranes.

Moreover, from Fig. 2b, it is obvious that the numbers of solvent molecules in TpPa-NH_2, TpPa-SO_3H and TpPa-COOH membranes are approximate, with slightly higher numbers observed in TpPa-H. The other two solvents (Fig. 2c&d) exhibit similar trend. The reason can be attributed to the larger pore size of TpPa-H compared to other three TpPa-R membranes that have different graft groups [39].

After figuring out the flow details of each solvent inside various TpPa-R membranes, we then investigate the transport mechanism of solvents in the mixed-solvent cases, namely methanol/ethanol and acetone/ethanol cases. In the mixed-solvent cases, the molar ratio of 1:1 is selected for binary solvents. Such molar ratio can reduce the error caused by the uneven local solvent concentration in the simulation and make the simulation results more representative. After performing the mixed-solvent simulations, flux results of each solvent in mixed-solvent cases are depicted in Fig. 3. Surprisingly, in both methanol/ethanol and acetone/ethanol cases, the fluxes of two components of solvents are obviously close. Notably, ethanol exhibits even higher flux than the other solvent in some TpPa-R membranes, sharply different from the

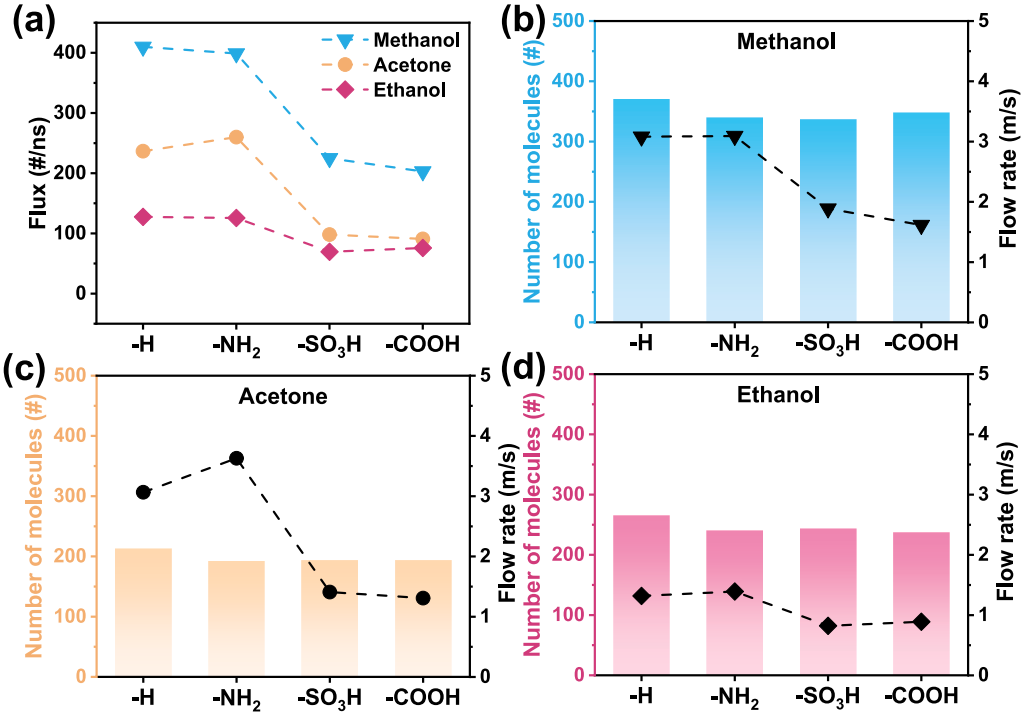

Fig. 2. (a) Fluxes of methanol, ethanol and acetone in TpPa-R membranes. The number of molecules of solvents inside TpPa-R membranes and their average flow rate of insides membranes: (b) methanol (c) acetone (d) ethanol.

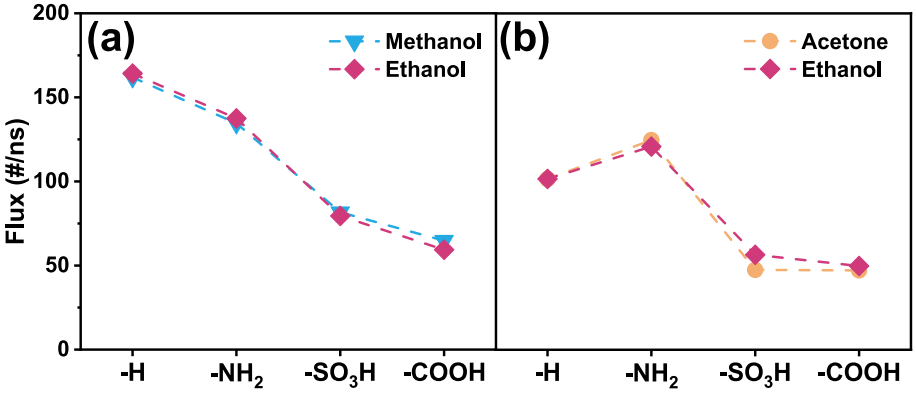

Fig. 3. Fluxes of two solvents and calculated real selectivity in the mixed-solvent cases: (a) methanol/ethanol (b) acetone/ethanol.

obviously lower flux of ethanol in pure-solvent case. In order to further reveal the reason behind such change of ethanol fluxes, we turn to compare the real selectivity and ideal selectivity in the coming section.

3.2. Ideal selectivity and real selectivity

For the binary mixed-solvent cases, the selectivity between different solvents can be calculated by the flux of the two solvent molecules and their compositions in mixed solvents:

$$S_{A/B} = \frac{F_A}{n_A} \Big/ \frac{F_B}{n_B} \tag{2}$$

where subscript 'A' and 'B' represent solvent A and solvent B respectively, F is molar flux of solvents, and n is molar fraction of solvents. For the pure-solvent simulation case, n_A and n_B are both 1, so Eq. (2) can be simplified as,

$$S_{A/B} = \frac{F_A}{F_B} \tag{3}$$

Since the molar ratio of two solvents in the mixed-solvent cases are all 1:1, indicating that n_A and n_B are both 0.5 for all mixed-solvent cases. Therefore, the real selectivity can be also calculated by Eq. (3).

The ideal selectivity (as shown in Fig. 4a) is calculated based on the above equation. It can be found that the ideal selectivity of acetone to ethanol in the TpPa-COOH case is 1.198, and the ideal selectivity of all other methanol or acetone to ethanol is significantly higher than 1.0, indicating that separation of methanol/ethanol (or acetone/ethanol) is practical.

According to the flux data of each solvent molecule in the mixed-solvent cases (shown in Fig. 3), the selectivity of each mixed-solvent case can be calculated. The real selectivity results are shown in Fig. 4b. It is evident that the real selectivity of methanol/ethanol is significantly lower than their respective ideal values and approximates 1.0. Similar results can be also observed for the cases of acetone/ethanol. These results suggest that ethanol molecules are hardly to be separated from methanol (or acetone) molecules through the TpPa-R membranes.

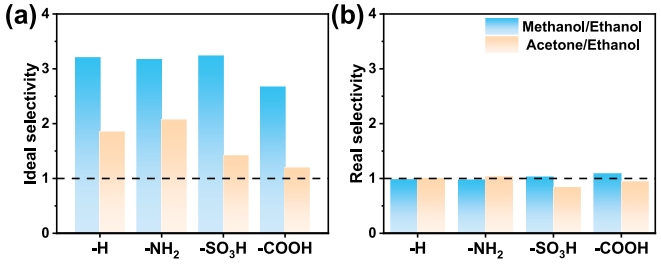

Fig. 4. The (a) ideal and (b) real selectivity of methanol and acetone to ethanol, respectively.

To explore the reasons behind the discrepancy between real and ideal selectivity, we then analyze transport processes of solvent molecules in both pure-solvent and mixed-solvent cases.

3.3. Analysis of pore-entrance sieving effect and in-pore transport effect

By considering both the pore-entrance sieving effect and the in-pore transport effect, it can be easier easily to understand the transport mechanisms of fluids through membranes [40,41]. The analysis of pore-entrance sieving and in-pore transport effects to solvent-separation systems are firstly applied in this work. The solvent selectivity based on its definition are recalculated to verify the rationality of the aforementioned selectivity calculation. For solvent molecules, their flux can be expressed as:

$$F_A = c_A \bullet v_A \tag{4}$$

where c_A represents the molar concentration of solvent A in the membrane and v_A is the flow velocity of solvent A inside membranes. Therefore, the real selectivity can be expressed as:

$$S_{A/B} = \frac{F_A}{F_B} = \frac{c_A v_A}{c_B v_B} = \frac{c_A}{c_B} \bullet \frac{v_A}{v_B} = \phi_c \bullet \phi_v \tag{5}$$

From Eq. (5), the real selectivity of solvent A for B can be calculated using pore-entrance sieving($\frac{c_A}{c_B}$) and in-pore transport($\frac{v_A}{v_B}$), which is represented by ϕ_c and ϕ_v, respectively. The data from Fig. 2b-d are applied to calculate c and v, and the calculated results of each component in Eq. (5) are listed in Table 1. S_ϕ is the calculated ideal selectivity of methanol to ethanol based on the data of ϕ_c and ϕ_v. Comparing the pure methanol and ethanol cases, it is observed that $\phi_{v,\,M/E}$ is close to 2.0. It suggests that the flow rate of methanol inside the membrane is approximately twice of ethanol's flow rate. Additionally, the generally higher values of $\phi_{c,\,M/E}$ indicate greater numbers of methanol molecules inside membranes over ethanol. In contrast, in the case of acetone/ethanol mixture, the larger molecular weight of acetone results in $\phi_{c,\,A/E}$ less than 1.0. However, $\phi_{v,\,A/E}$ is obviously larger than 1.0 because of acetone's higher flow rate inside the membranes, thereby yielding the ideal selectivity of

Table 1
Pore-entrance sieving(ϕ_c), in-pore transport(ϕ_v) and the calculated ideal selectivity (S_ϕ) based on Eq.5 for pure-solvent cases.

COFs	TpPa-H	TpPa-NH_2	TpPa-SO_3H	TpPa-COOH
$\phi_{c,\,M/E}$	1.394	1.414	1.384	1.463
$\phi_{v,\,M/E}$	2.338	2.223	2.298	1.814
$S_{\phi,\,M/E}$	3.260	3.144	3.181	2.654
$\phi_{c,\,A/E}$	0.802	0.801	0.790	0.810
$\phi_{v,\,A/E}$	2.325	2.609	1.714	1.469
$S_{\phi,\,A/E}$	1.864	2.089	1.355	1.191

acetone to ethanol ($S_{\phi,\ A/E}$) larger than 1.0. Compared with the calculated ideal selectivity (S_{ϕ}) results based on fluxes, it can be found that S_{ϕ} values are highly consistent with those in Fig. 4. This proves the rationality of our analysis on pore-entrance sieving and in-pore transport effects on the membrane separation of solvents.

With the success of analysis on pore-entrance sieving and in-pore transport effects, we prefer to calculating the S_{ϕ}, ϕ_c and ϕ_v for the mixed-solvent cases. Before that, we need to obtain the number of solvent molecules in the membrane and their flow rates, which are plotted in Fig. 5. It is found that the number of molecules of all solvents in the pore decreases significantly compared to the cases of pure solvents. For instance, in the TpPa-H membrane, the number of methanol molecules decreases from 369 for pure methanol cases to 160 for the methanol/ethanol mixture. This reduction occurs because ethanol molecules occupy an almost half portion of the pore space after mixing, displacing methanol molecules from their original positions.

Additionally, in each mixed-solvent cases, the gaps of the number of molecules between the two solvents is notably reduced compared to pure solvent cases. Furthermore, it is also observed that the flow rates of mixed solvents inside the membrane are similar, which is inconsistent with the results obtained in the pure-solvent cases. Therefore, it is necessary to perform the analysis on the pore-entrance sieving and in-pore transport effects for the mixed-solvent cases.

The calculated S_{ϕ}, ϕ_c and ϕ_v for the mixed-solvent cases are provided in Table 2. It is observed that all ϕ_c components of mixed-solvent cases are closer to 1, which differs from those of pure-solvent cases. The interactions of solvents with TpPa-R are calculated (listed in Table S1). For each TpPa-R, the interactions of three types of solvents are close, resulting in the similar ϕ_c values of mixed-solvent cases. Moreover, the similar interactions also demonstrate that the variation of ϕ_c is mainly due to the molecular size. The results above indicate a diminished sieving effect at the pore mouth, thus exerting a minor influence on selectivity in mixed-solvent cases. Additionally, the in-pore transport coefficients (ϕ_v) in all mixed-solvent cases are also approximately 1. It implies that the relative flow rate of methanol (or acetone) to ethanol decreases obviously. The transport resistance of ethanol and another two solvents in those membranes is similar at this time. Therefore, it can be considered that the effect of the graft groups in the TpPa-R membrane on the transport process of solvent molecules is weak and neglectable in the mixed-solvent cases.

Table 2
Calculated pore-entrance sieving(ϕ_c), in-pore transport(ϕ_v) values in mixed-solvent cases.

COFs	$\phi_{c,\ M/E}$	$\phi_{v,\ M/E}$	$\phi_{c,\ A/E}$	$\phi_{v,\ A/E}$
TpPa-H	1.114	0.930	0.936	1.138
TpPa-NH_2	1.094	0.943	0.876	1.151
TpPa-SO_3H	1.064	0.944	0.812	1.096
TpPa-COOH	1.142	0.868	1.175	0.808

Since TpPa-R membranes have pore size larger than the molecular size of all three solvents in this work, the diminished pore-entrance sieving effect is expectable. However, the proximal intramembrane flow rates of two solvents in the mixed-solvent cases are out of expectation. Therefore, we will focus on the flow rates of all solvents inside membranes.

In the binary mixed-solvent cases, similar flow rates of two species typically arise from conditions where one species' slower flow impedes the transport of faster species. For example, the existence of ions inside nanopores of membranes will somehow block the nanopores and hinder the transport of water molecules inside nanopores [42,43]. In this study, it is likely that the flow rates of methanol or acetone molecules is impeded by ethanol molecules, leading to a decrease in the value of ϕ_v. Therefore, the flow rates of each solvent in the mixed-solvent cases are

Table 3
The ratios of the flow rates in the mixed-solvent and pure-solvent cases v_m/v_p for each kind of solvents.

COFs	Methanol	Acetone	Ethanol	
			mixed with methanol	mixed with acetone
TpPa-H	0.921	0.860	2.316	1.757
TpPa-NH_2	0.836	0.906	1.972	2.055
TpPa-SO_3H	0.862	0.957	1.413	1.497
TpPa-COOH	0.677	0.870	2.100	1.583

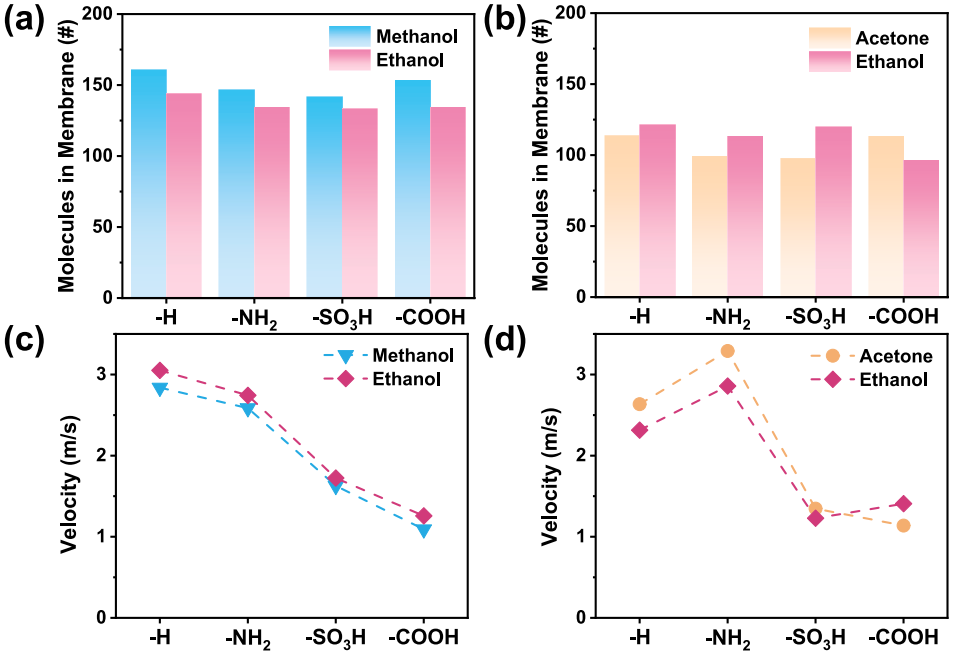

Fig. 5. The number of molecules for the two solvents in the membrane in the case of (a) methanol/ethanol (b) acetone/ethanol. The flow rates of molecules for two solvents inside membranes in the case of (c) methanol/ethanol and (d) acetone/ethanol.

calculated and the ratios of their flow rates before (v_p) and after mixing (v_m) are listed in Table 3. It is evident that the ratios of v_m/v_p for methanol or acetone are close to 1.0, indicating that the flow rates of methanol or acetone molecules did not exhibit a significant decrease while being mixed with ethanol. Conversely, the flow rates of ethanol undergo a significant promotion in the mixed-solvent cases. In some cases, it exhibits a promotion of over 100 %.

Based on the above analysis, the decrease in real selectivity of mixed solvent cases compared to ideal selectivity is primarily attributed to changes in the flow rate of solvent molecules inside the membrane (in-pore transport effect), rather than differences in molecular density inside membranes (pore-entrance sieving effect). Specifically, the reduced selectivity in mixed-solvent cases is due to a significantly increased flow rates of ethanol molecules. Therefore, it is necessary to unveil the reason behind the increase of flow rates for ethanol.

3.4. Interactions between solvents and TpPa-R pore walls

In the work of Qin *et al.*, the existence of ethanol molecules inside slit nanopores resulted in the preferential adsorption of ethanol onto pore walls. The adsorption of ethanol reduces the opportunity of water molecules forming hydrogen bonds with pore wall and thus promote the water permeance [44]. In this work, the increased ethanol's flow rates might originate from the preferential adsorption of methanol or acetone to the pore wall of COFs in the mixed-solvent cases. The hydrophilic group of methanol or acetone can form hydrogen bonds with polar groups (such as oxygen atoms) on the TpPa-R pore walls. Meanwhile, the hydrophobic end orients towards the pore center, thereby emerging a hydrophobic pore wall. This will reduce the transport resistance of ethanol within the hydrophobic channel, and thereby accelerate its transport.

To investigate the preferential adsorption of methanol and acetone molecules on TpPa-R pore walls, we first examine the spatial distribution of oxygen atoms from three solvents: methanol, ethanol, and acetone, on the pores (shown in Fig. 6). It is observed that in the methanol/ethanol cases, both methanol and ethanol exhibit similar adsorption sites on the oxygen atoms of the TpPa-H pore walls. There is no significant difference in the frequency of solvent molecules at these adsorption sites, suggesting similar adsorption capacities for methanol and ethanol on the pore walls. In the acetone/ethanol cases, ethanol shows a higher density at the adsorption sites compared to acetone in TpPa channels.

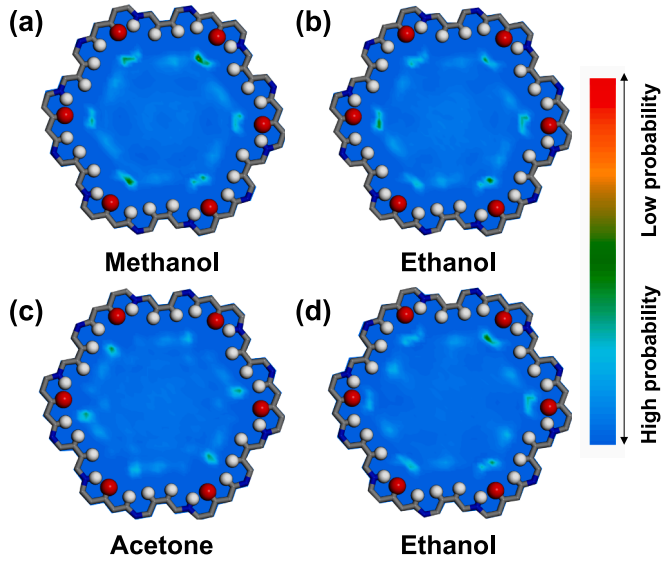

Fig. 6. The density distribution of two solvents in mixed-solvent cases: (a) methanol, (b) ethanol in methanol/ethanol cases and (c) acetone, (d) ethanol in acetone/ethanol cases. The color from blue to red indicates the molecular density of solvents from low to high. (For interpretation of the references to color in this figure legend, the reader is referred to the web version of this article.)

The radial density distribution of the polar groups on TpPa-R pore walls with solvents will further investigate whether there is preferential adsorption of methanol (or acetone) onto pore walls. From Fig. 7a, it is found that the peaks of methanol and ethanol are both near 7 Å, which is also observed in the case of methanol with polar pore wall of zeolites [45]. In the cases of acetone/ethanol, we obtain similar conclusion, indicating that both solvents are equally distributed at the pore wall. No preferential adsorption of methanol (or acetone) onto pore walls is observed. The results from Fig. 7 also indicate that the interaction of TpPa-R membranes with all three solvents are similar. Therefore, no solvent will preferentially enter the nanopores of TpPa-R membranes, resulting in the same opportunity of entrance for all three solvents. This conclusion can be validated by the values of ϕ_c being around 1.0 for mixed-solvent cases in the previous sections.

3.5. Diffusion properties of mixed solvents

In the previous sections, the influence of TpPa-R pore walls on the transport of solvents are excluded from the reason of flow-rate promotion of ethanol. The reason should be further explored. Rather than solvent-pore wall interactions, there is solvent–solvent interactions for the mixed-solvent cases. We then focus on the mobility of each solvent before and after mixing. Mean square displacement (MSD) of molecules is usually calculated to represent the molecular mobility in MD simulations. Subsequently, the self-diffusion coefficients of each molecule can be calculated based on the curves of MSD.

MSD is a function describing the displacement of particles with time [46]. To conduct MSD analysis, five additional cases containing only solvent molecules are constructed in this study: methanol, acetone, ethanol, methanol/ethanol, and acetone/ethanol cases. The NPT process parameters are consistent with previous setups. Subsequently, a 4 ns NVT process (without external forces) is conducted to simulate the mobility behavior of solvent molecules undisturbed by external influences, maintaining the system temperature at 300 K [47]. According to the definition of MSD:

$$\mathrm{MSD}(t) = |r(t) - r(0)|^2 \tag{6}$$

where $r(t)$ is the spatial position of the target atom at time t; $r(0)$ represents the initial position of the target atom. The self-compiled code calculates the cumulative squared displacement of the target atom at various time intervals while considering periodic boundary effects, and normalizes it to obtain the MSD.

In this study, the self-diffusion coefficient (D) is used to characterize the dynamics of molecules. D can be calculated using the following expression:

$$D = \frac{\lim_{t\to 0}\mathrm{MSD}(t)}{6t} \tag{7}$$

The MSD curves for various solvents are shown in Fig. S2. Each MSD curve exhibits notably linear and the slopes of these lines represent their respective D values. Finally, the D results of each solvent are shown in Fig. 8. From Fig. 8a, methanol and acetone demonstrate similar values of D, notably larger than that of ethanol. In Fig. 8b&c, ethanol's D value is close to that of methanol and acetone. Comparing Fig. 8b&c with 8a, it is easy to find that methanol and acetone exhibit a slight decrease in D values while ethanol's D value sharply increases to that of the other solvents in each binary mixed-solvent cases. Such promotion of ethanol's D value reflects the changes in its mobility inside the nanopores.

To further figure out the reason for the promotion of ethanol's mobility in mixed-solvent cases, we calculated the interactions between ethanol molecules when they are in pure- and mixed-solvent cases

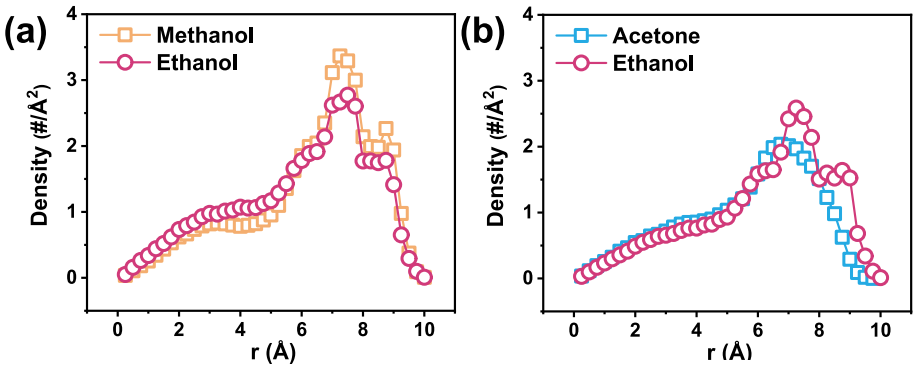

Fig. 7. (a) Density profiles of two solvents in methanol/ethanol case along the radial direction ; (b) Density profiles of two solvents in acetone/ethanol case along the radial direction.

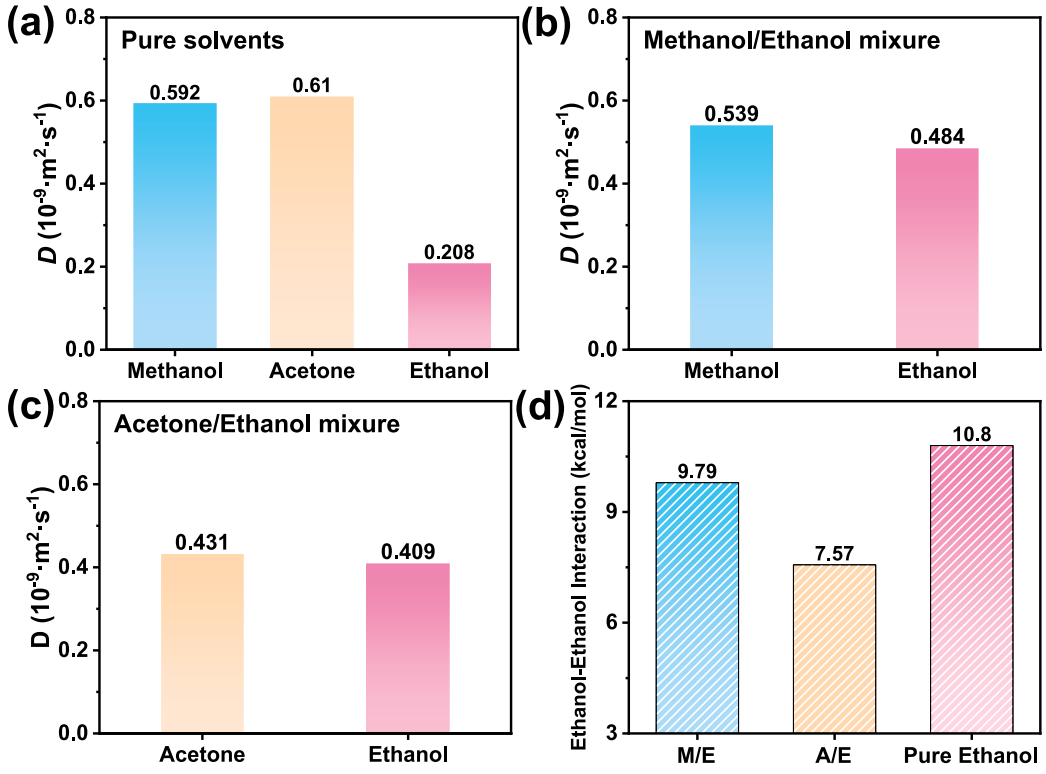

Fig. 8. Self-diffusion coefficients (*D*) of solvent molecules in (a) pure solvent cases, and those in mixed-solvent cases: (b) methanol/ethanol and (c) acetone/ethanol. (d) Ethanol-ethanol interactions in mixed- and pure-solvent cases. M/E and A/E indicate the methanol/ethanol and acetone/ethanol mixtures, respectively.

(shown in Fig. 8d). It is evidently that the ethanol-ethanol interaction is obvious higher in pure-solvent case than those in mixed-solvent cases. Such higher value results in the strong attraction between ethanol molecules in pure ethanol solvent. When they are moved into mixed-solvent cases, the attraction between ethanol molecules is obviously reduced and thus the mobility of ethanol is promoted. This finding reminds us that unlike desalination or liquid–solid separation systems, interactions between solvents play a crucial role in determining separation performance in the solvent separation systems.

4. Conclusion

In this study, molecular dynamics simulations are employed to investigate the separation of binary solvents (methanol/ethanol and acetone/ethanol). The simulation results reveal that while the ideal selectivity of several cases is far over 1, their real selectivity drops to near 1. To figure out the reason behind, we preform the analysis of pore-entrance sieving and in-pore transport effect. The results indicate that the decrease in real selectivity is primarily attributed to in-pore transport effect, without preferential entry of ethanol molecules into the membrane pores. Moreover, the analysis of in-pore transport effect demonstrates the relatively higher ethanol flow rates compared to methanol or acetone in mixed-solvent cases. Compared to the pure-solvent cases, a significant promotion of flow rate for ethanol, rather than the dropped flow rates of methanol or acetone, is observed in mixed-solvent cases. Density distribution and radial density distribution of different solvents inside the nanopores indicate that methanol and acetone did not preferentially adsorb onto the COF. This suggests a weak correlation of the microstructure of solvent molecules inside the TpPa-R nanopores. Furthermore, self-diffusion coefficient (*D*) results in pure- and mixed-solvent cases reveal that ethanol's *D* values increase to the levels similar to those of the other solvents in binary solvent mixtures. The promoted *D* of ethanol in mixed-solvent cases should be attributed to the reduced interactions between ethanol molecules because of the

coexistence of other solvent molecules. This work is expected to provide insights and guidance for the rational design of next-generation nanofiltration membranes for solvent separations.

Author contributions.

Shukai Li: Investigation, Data curation, Writing – original draft. **Bowen Liu:** Investigation, Methodology. **Mingjie Wei:** Validation, Writing – review & editing, Funding Acquisition. **Ming Liu:** Writing-review. **Jinji Cao:** Methodology, Validation. **Weihong Xing:** Supervision. **Yong Wang:** Conceptualization, Writing – review & editing, Supervision, Funding Acquisition.

Declaration of competing interest

The authors declare that they have no known competing financial interests or personal relationships that could have appeared to influence the work reported in this paper.

Data availability

Data will be made available on request.

Acknowledgement

This work was financially supported by the National Key Research and Development Program of China (2022YFB3805201) and the National Natural Science Foundation of China (21921006). The authors also thank the High Performance Computing Centre of Nanjing Tech University for supporting the computational resources.

References

[1] D.S. Sholl, R.P. Lively, Seven chemical separations to change the world, Nature 532 (7600) (2016) 435–437, https://doi.org/10.1038/532435a.
[2] M. Miceli, P. Frontera, A. Macario, A. Malara, Recovery/reuse of heterogeneous supported spent catalysts, Catalysts 11 (5) (2021) 17, https://doi.org/10.3390/catal11050591.
[3] L. Huang, J. Chen, T. Gao, M. Zhang, Y. Li, L. Dai, L. Qu, G. Shi, Reduced graphene oxide membranes for ultrafast organic solvent nanofiltration, Adv. Mater 28 (39) (2016) 8669–8674, https://doi.org/10.1002/adma.201601606.
[4] P. Marchetti, M.F. Jimenez Solomon, G. Szekely, A.G. Livingston, Molecular separation with organic solvent nanofiltration: a critical review, Chem. Rev. 114 (21) (2014) 10735-10806. DOI: 10.1021/cr500006j.
[5] M. Buonomenna, J. Bae, Organic solvent nanofiltration in pharmaceutical industry, Sep. Purif. Rev. 44 (2) (2015) 157–182, https://doi.org/10.1080/15422119.2014.918884.
[6] S. Ali, I.A. Shah, I. Ihsanullah, X. Feng, Nanocomposite membranes for organic solvent nanofiltration: Recent advances, challenges, and prospects, Chemosphere 308 (2022) 177–206, https://doi.org/10.1016/j.chemosphere.2022.136329.
[7] R. Abejón, A. Garea, A. Irabien, Organic solvent recovery and reuse in pharmaceutical purification processes by nanofiltration membrane cascades, Chemical Engineering Transactions (43) (2015) 1057–1062, https://doi.org/10.3303/CET1543177.
[8] Y. Lu, W. Liu, J. Liu, X. Li, S. Zhang, A review on 2D porous organic polymers for membrane-based separations: Processing and engineering of transport channels, Advanced Membranes 1 (2021) 100014, https://doi.org/10.1016/j.advmem.2021.100014.
[9] X.Q. Cheng, Y.L. Zhang, Z.X. Wang, Z.H. Guo, Y.P. Bai, L. Shao, Recent advances in polymeric solvent-resistant nanofiltration membranes, Adv. Polym. Technol. 33 (S1) (2014) 24, https://doi.org/10.1002/adv.21455.
[10] B. Zhao, G.M. Shi, J.-Y. Lai, T.-S. Chung, Braid-reinforced polybenzimidazole (PBI) hollow fiber membranes for organic solvent nanofiltration (OSN), Sep. Purif. Technol. 290 (2022) 11, https://doi.org/10.1016/j.seppur.2022.120811.
[11] W. Wei, J. Liu, J. Jiang, Computational design of 2D covalent-organic framework membranes for organic solvent nanofiltration, ACS Sustainable Chem. Eng. 7 (1) (2018) 1734–1744, https://doi.org/10.1021/acssuschemeng.8b05599.
[12] Z. Wang, X. Luo, J. Zhang, F. Zhang, W. Fang, J. Jin, Polymer membranes for organic solvent nanofiltration: Recent progress, challenges and perspectives, Advanced Membranes 3 (2023) 100063, https://doi.org/10.1016/j.advmem.2023.100063.
[13] L. Zhang, J. Wang, Y. Zhang, J. Zhu, J. Yang, J. Wang, Y. Zhang, Y. Wang, Leaf-veins-inspired nickel phosphate nanotubes-reduced graphene oxide composite membranes for ultrafast organic solvent nanofiltration, J. Membr. Sci. 649 (2022) 11, https://doi.org/10.1016/j.memsci.2022.120401.
[14] T. Rasheed, S. Khan, T. Ahmad, N. Ullah, Covalent organic frameworks-based membranes as promising modalities from preparation to separation applications: an overview, Chem Rec 22 (8) (2022) 27, https://doi.org/10.1002/tcr.202200062.
[15] J. Li, X. Zhou, J. Wang, X. Li, Two-dimensional covalent organic frameworks (COFs) for membrane separation: a mini review, Ind Eng Chem Res 58 (34) (2019) 15394–15406, https://doi.org/10.1021/acs.iecr.9b02708.
[16] S. Yuan, X. Li, J. Zhu, G. Zhang, P. Van Puyvelde, B. Van der Bruggen, Covalent organic frameworks for membrane separation, Chem. Soc. Rev. 48 (10) (2019) 2665–2681, https://doi.org/10.1039/c8cs00919h.
[17] B. Mishra, B.P. Tripathi, Flexible covalent organic framework membranes with linear aliphatic amines for enhanced organic solvent nanofiltration, J. Mater. Chem. A 11 (30) (2023) 16321–16333, https://doi.org/10.1039/d3ta02683c.
[18] Y. Yin, S. Liu, J. Zhou, Y. Peng, E. Wang, L. Han, B. Su, Polyamide thin film nanocomposite with in-situ co-constructed COFs for organic solvent nanofiltration, J. Membr. Sci. 686 (2023) 13, https://doi.org/10.2139/ssrn.4462915.
[19] X. Zhu, B. Ma, Y.Q. Ai, L. Zhang, X.P. Wang, L.J. Liang, J.W. Shen, Investigation on dye separation mechanism in covalent-organic framework membranes with molecular dynamics simulation, Microporous Mesoporous Mater. 349 (2023) 13, https://doi.org/10.1016/j.micromeso.2022.112417.
[20] Y.Q. Zhang, J. Guo, G. Han, Y.P. Bai, Q.C. Ge, J. Ma, C.H. Lau, L. Shao, Molecularly soldered covalent organic frameworks for ultrafast precision sieving, Sci. Adv. 7 (13) (2021) 9, https://doi.org/10.1126/sciadv.abe8706.
[21] M. Dahanayaka, J.W. Chew, Organic solvent permeation through negatively charged graphene oxide membranes, ACS Sustainable Chem. Eng. 10 (4) (2022) 1499–1508. DOI: acssuschemeng.1c06824.
[22] F. Xu, M. Wei, Y. Wang, Effect of hydrophilicity on ion rejection of sub-nanometer pores, Sep. Purif. Technol. 257 (2021) 8, https://doi.org/10.1016/j.seppur.2020.117937.
[23] Y.H. Wang, W.H. Wang, Z.Q. Zhang, P. Li, Adsorption performance of the functional COFs for removal of bisphenol A: Molecular dynamic simulations, J. Mol. Liq. 392 (2023) 10, https://doi.org/10.1016/j.molliq.2023.123475.
[24] J.Q. Yuan, X.D. You, N.A. Khan, R.L. Li, R.N. Zhang, J.L. Shen, L. Cao, M.Y. Long, Y.A. Liu, Z.J. Xu, H. Wu, Z.Y. Jiang, Photo-tailored heterocrystalline covalent organic framework membranes for organics separation, Nat. Commun. 13 (1) (2022) 7, https://doi.org/10.1038/s41467-022-31361-w.
[25] A.P. Thompson, H.M. Aktulga, R. Berger, D.S. Bolintineanu, W.M. Brown, P.S. Crozier, P.J. In't Veld, A. Kohlmeyer, S.G. Moore, T.D. Nguyen, LAMMPS-a flexible simulation tool for particle-based materials modeling at the atomic, meso, and continuum scales, Comput. Phys. Commun. 271 (2022) 34. DOI: 10.1016/j.cpc.2021.108171.
[26] J. Lenhard, S. Stephan, H. Hasse, On the History of the Lennard-Jones Potential, Ann. Phys. 536 (6) (2024) 4, https://doi.org/10.1002/andp.202400115.
[27] S.L. Mayo, B.D. Olafson, W.A. Goddard, DREIDING: a generic force field for molecular simulations, J. Phys. Chem. 94 (26) (1990) 8897–8909, https://doi.org/10.1021/j100389a010.
[28] W. Zhou, M.J. Wei, X. Zhang, F. Xu, Y. Wang, Fast Desalination by Multilayered Covalent Organic Framework (COF) Nanosheets, ACS Appl. Mater. Interfaces 11 (18) (2019) 16847–16854, https://doi.org/10.1021/acsami.9b01883.
[29] M.J. Guan, D.F. Yang, Q. Li, H.T. Zhang, J.A. Xu, M.M. Cai, W.K. Lin, S.Q. Ma, Q. Z. Liu, Desalination behavior of composite membrane with petal shaped pore-formed by superimposition of covalent organic framework with large aperture difference, Appl. Surf. Sci. 616 (2023) 10, https://doi.org/10.1016/j.apsusc.2023.156441.
[30] J.X. Liu, X.H. Liu, W.Q. Tao, Z. Li, H. Xu, Understanding of water desalination in two-dimensional porous membrane via molecular dynamics, J. Mol. Liq. 360 (2022) 8, https://doi.org/10.1016/j.molliq.2022.1194080.
[31] W.D. Cornell, P. Cieplak, C.I. Bayly, I.R. Gould, K.M. Merz, D.M. Ferguson, D. C. Spellmeyer, T. Fox, J.W. Caldwell, P.A. Kollman, A second generation force field for the simulation of proteins, nucleic acids, and organic molecules, J Am Chem Soc 117 (19) (1995) 5179–5197, https://doi.org/10.1021/ja00124a002.
[32] A.K. Rappe, W.A. Goddard III, Charge equilibration for molecular dynamics simulations, J. Phys. Chem. 95 (8) (1991) 3358–3363, https://doi.org/10.1021/j100161a070.
[33] M. Schauperl, P.S. Nerenberg, H. Jang, L.-P. Wang, C.I. Bayly, D.L. Mobley, M. K. Gilson, Non-bonded force field model with advanced restrained electrostatic potential charges (RESP2), Commun. Chem. 3 (1) (2020) 44, https://doi.org/10.1038/s42004-020-0291-4.
[34] T. Lu, F. Chen, Multiwfn: A multifunctional wavefunction analyzer, J. Comput. Chem. 33 (5) (2012) 580–592, https://doi.org/10.1002/jcc.22885.
[35] T.F. Willems, C. Rycroft, M. Kazi, J.C. Meza, M. Haranczyk, Algorithms and tools for high-throughput geometry-based analysis of crystalline porous materials, Microporous Mesoporous Mater. 149 (1) (2012) 134–141, https://doi.org/10.1016/j.micromeso.2011.08.020.
[36] Y. Song, M. Wei, F. Xu, Y. Wang, Molecular simulations of water transport resistance in polyamide RO membranes: interfacial and interior contributions, Engineering 6 (5) (2020) 577–584, https://doi.org/10.1016/j.eng.2020.03.008.
[37] X. Zhang, M.J. Wei, F. Xu, Y. Wang, Thickness-dependent ion rejection in nanopores, J. Membr. Sci. 601 (2020) 6, https://doi.org/10.1016/j.memsci.2020.117899.
[38] X. Zhang, M. Wei, Y. Wang, Designing sub-nanometer pores for efficient boron removal, Desalination 533 (2022) 9, https://doi.org/10.1016/j.desal.2022.115755.
[39] K.M. Gupta, S. Aitipamula, P.S. Chow, In-silico design of covalent organic framework membranes for efficient water/ethanol separation, J. Membr. Sci. 687 (2023) 9, https://doi.org/10.1016/j.memsci.2023.122083.
[40] D.C. Liao, Z.Q. Xu, M.J. Wei, Y. Wang, Interference mechanism of cations on transport of lithium and magnesium inside COF nanofiltration membranes, Mol. Simul. 48 (15) (2022) 1369–1377, https://doi.org/10.1080/08927022.2022.2094372.

[41] F. Xu, M. Wei, X. Zhang, Y. Wang, Ion rejection in covalent organic frameworks: revealing the overlooked effect of in-pore transport, ACS Appl. Mater. Interfaces 11 (48) (2019) 45246–45255, https://doi.org/10.1021/acsami.9b18234.
[42] Y. Gaganpreet, Pathania, Charged nanoporous phosphorene as a water desalination membrane: insights from molecular dynamics, Nanotechnology 35 (4) (2024) 10, https://doi.org/10.1088/1361-6528/ad0504.
[43] L.L. Qin, H.O. Huang, J. Zhou, Modulation of ion transport through nanopores in water desalination: a molecular dynamics study, Mol. Simul. (2023) 16, https://doi.org/10.1080/08927022.2023.2268205.
[44] Y. Qin, N. Zhao, Y. Zhu, Y. Zhang, Q. Gao, Z. Dai, Y. You, X. Lu, Molecular insights into the microstructure of ethanol/water binary mixtures confined within typical 2D nanoslits: The role of the adsorbed layers induced by different solid surfaces, Fluid Phase Equilib. 509 (2020) 8, https://doi.org/10.1016/j.fluid.2019.112452.
[45] Y.B. Tang, S.J. Xie, Structure and dynamics of a water/methanol mixture confined in zeolitic imidazolate framework ZIF-8 from atomistic simulations, Phys Chem Chem Phys 24 (8) (2022) 5220–5232, https://doi.org/10.1039/d1cp05571b.
[46] X. Michalet, Mean square displacement analysis of single-particle trajectories with localization error: Brownian motion in an isotropic medium, Phys. Rev. E 82 (4) (2010) 13, https://doi.org/10.1103/PhysRevE.82.041914.
[47] M. Kialashaki, J.S. Amin, S. Zendehboudi, Molecular dynamics simulation to evaluate the stability of tetra-n-butyl ammonium/phosphonium bromide semiclathrate hydrates in the presence and absence of methane, carbon dioxide, methanol, and ethanol molecules, Ind. Eng. Chem. Res. 62 (18) (2023) 7175–7196, https://doi.org/10.1021/acs.iecr.3c00375.